

Four-wave-mixing measurements of energy migration and radiationless relaxation processes in alexandrite crystals

Andrzej Suchocki, Guy D. Gilliland, and Richard C. Powell

Department of Physics, Oklahoma State University, Stillwater, Oklahoma 74078-0444

(Received 12 May 1986; revised manuscript received 18 August 1986)

Four-wave-mixing techniques were used to establish and probe population gratings of Cr^{3+} ions in both mirror and inversion sites in $\text{BeAl}_2\text{O}_4:\text{Cr}^{3+}$ crystals as a function of temperature between about 6 and 300 K. The four-wave-mixing signal intensity and decay rate were monitored as a function of the crossing angle of the laser "write" beams. The variation of the signal intensity with crossing angle is explained theoretically with use of a model based on the interaction between the laser and a two-level atomic system. Theoretical fits to the results provide information concerning the relative importance of the absorption and dispersion contributions to the signal, and the dephasing time of the atomic system. The latter is found to be 2.2 psec for the mirror site ions and 80 psec for the inversion site ions. The signal decay rate of the inversion site ions was found to be independent of crossing angle at all temperatures, while the signal decay rate for ions in the mirror site increased with increasing crossing angle at temperatures below about 150 K. This indicates the presence of long-range energy migration, and the diffusion coefficient describing this process was found to increase to about $4.2 \times 10^{-7} \text{ cm}^2 \text{ sec}^{-1}$ at 6 K.

I. INTRODUCTION

The optical properties of alexandrite ($\text{BeAl}_2\text{O}_4:\text{Cr}^{3+}$) are of interest because of its importance as a tunable solid-state laser material.¹ We have recently reported some of the optical-spectroscopic properties of alexandrite, including the results of four-wave-mixing (FWM) measurements at room temperature.²⁻⁴ In this paper we describe the results of extending our FWM measurements to low temperatures.

The mechanism of transient FWM in doped crystals is scattering from a laser-induced population grating. In alexandrite the Cr^{3+} ions can occupy two nonequivalent crystal-field sites, one having mirror symmetry and the other inversion symmetry. We have shown previously that population gratings can be established for Cr^{3+} ions in either type of site.⁴ The grating can be associated with differences in either the absorption or dispersion properties of the Cr^{3+} ions when they are in the excited state instead of the ground state. We describe here a method for determining the contributions to the FWM signal from these two types of refractive-index modulation. The ratio of these two contributions is used to determine the dephasing time T_2 of the Cr^{3+} ions interacting with the laser excitation. For the experimental conditions used here, the dominant process in the dephasing is the pump-band-to-metastable-state radiationless relaxation process, which is of interest in understanding laser-pumping dynamics.

The transient dynamics of the FWM signal can be used to characterize the properties of energy migration among ions in crystals if the migration distance is of the order of the peak-to-valley separation of the laser-induced grating.⁵⁻⁷ Our previous FWM results showed that no long-range energy transfer was taking place among the Cr^{3+} ions in alexandrite at room temperature.⁴ This remains

true for inversion-site ions at low temperatures. However, for ions in the mirror sites, the influence of long-range energy transfer on the FWM signal decay becomes evident below 150 K. The diffusion coefficient determined from these measurements increases to a value of $4.2 \times 10^{-7} \text{ cm}^2 \text{ sec}^{-1}$ at 6 K. This surprising result may be associated with nonuniform Cr^{3+} -ion distributions which are known to be present in alexandrite.²

II. EXPERIMENTAL APPARATUS AND SAMPLES

The crystal used for this work was an oriented cube of $\text{BeAl}_2\text{O}_4:\text{Cr}^{3+}$ with each edge measuring approximately 7 mm. The concentration of Cr^{3+} ions is 0.0325 at.%. The Cr^{3+} ions enter the lattice substitutionally for the Al^{3+} ions, which occur in the chrysoberyl structure with octahedral coordination of oxygen ions. They can occupy two inequivalent types of crystal-field sites, one with mirror symmetry belonging to the C_s point group and one with inversion symmetry belonging to the C_i point group. It has been found previously that 78% of the Cr^{3+} ions occupy mirror sites and 22% inversion sites.¹ The mirror-site ions dominate the optical spectroscopy and lasing properties of the material.

The experimental setup used for the nondegenerate FWM measurements is shown schematically in Fig. 1. For temperature control, the sample was mounted in either a cryogenic refrigerator or a liquid-helium Dewar. The laser excitation was provided by either the 488.0-nm output from an argon laser or the output of a ring dye laser with Rhodamine-6(G) dye tuned to 589.0 nm. The former selectively excites the ions in the inversion sites while the latter selectively excites ions in the mirror sites.² The laser output was split with a beam splitter into two beams of equal power (write beams) which travel equal path lengths before crossing at an angle θ inside the sam-

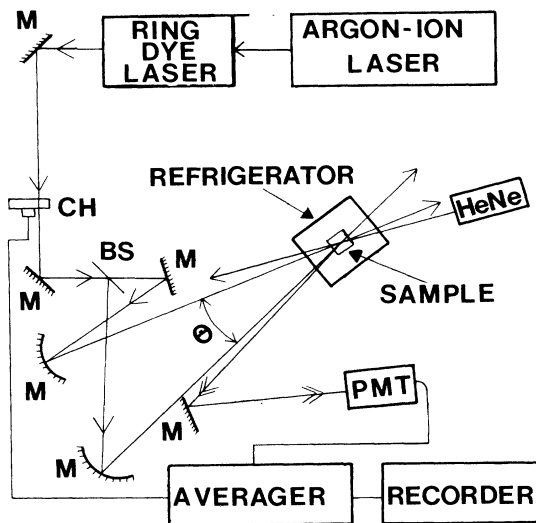


FIG. 1. Schematic representation of experimental apparatus for four-wave mixing. CH, chopper; PMT, photomultiplier tube; M, mirror; BS, beam splitter.

ple. Their interference forms a sinusoidal pattern which creates a spatial distribution of Cr^{3+} ions in the excited state with the same pattern. Due to the difference in the complex dielectric constant when the Cr^{3+} ions are in the ground and excited states, this population distribution acts as an index-of-refraction grating. Although the heat generated under these experimental conditions can also produce a change in the refractive index, thermal gratings have different magnitudes and angular dependences of the decay rates than population gratings. Thus it is easily possible to distinguish between contributions to the FWM signal from the two types of gratings. The properties of the FWM signal described in the following section show that the results reported here are associated with scattering from a population grating. No effects attributable to a thermal grating were observed. For nondegenerate FWM a He-Ne laser was used for a "read beam." This was aligned so it is almost counterpropagating to one of the write beams. It scatters from the index-of-refraction grating and produces a FWM signal leaving the sample almost counterpropagating to the other write beam. The signal beam was detected by an Amperex 2254B photomultiplier tube. To measure the intensity of the scattered light, the read beam was modulated with a mechanical chopper and an EG&G/PAR lock-in amplifier was used to enhance the signal-to-noise ratio. The decay rate of the signal was measured by chopping the write beams and storing the transient signal in an EG&G/PAR 4202 signal averager.

III. FWM STUDIES OF ENERGY TRANSFER

The decay of a FWM signal associated with a transient population grating is predicted to be a single exponential with a decay rate given by⁵

$$K = 2\tau^{-1} + [32(\pi/\lambda)^2 \sin^2(\theta/2)]D. \quad (1)$$

The first term describes the destruction of the grating due to the fluorescence decay of the ions in the excited state with a decay time of τ . The second term describes the destruction of the grating due to the migration of the excitation energy from ions in the peak to ions in the valley region of the grating. The latter term depends on the diffusion coefficient of the energy migration, D , and on the grating spacing $\Lambda = \lambda/[2 \sin(\theta/2)]$, where λ and θ are the wavelength and crossing angle of the laser write beams in the crystal, respectively. Thus by measuring the FWM signal decay rate as a function of the write-beam crossing angle, it is possible to determine the energy-diffusion coefficient.

A. Experimental results

For gratings selectively established with Cr^{3+} ions in inversion sites, no angular variation was observed for the FWM signal decay rate at any temperature. Typical results are shown in Fig. 2. The signals were exponential and decayed with half the fluorescence lifetime of inversion-site ions, as measured independently.²⁻⁴ This indicates that for Cr^{3+} ions in the inversion sites energy transfer does not take place over distances of the order of the grating spacing.

For gratings selectively established with Cr^{3+} ions in mirror sites, the FWM transient signals were nonexponential. A typical example is shown in Fig. 3. The decay rate of the long-time portion of the curve is equal to twice the fluorescence decay rate of the inversion-site ions. This long-time decay rate is independent of the write-beam crossing angle and power. Thus the long-time part of the nonexponential decay is associated with a population grating established with inversion-site ions due to energy transfer from mirror-site ions. In order to obtain an accurate decay rate for the mirror-site grating, the long-time decay curve is extrapolated to short times and subtracted from the measured curve as shown in Fig. 3. Although this procedure for separating the contributions to the signal due to the two types of gratings is not strictly correct for the case of energy transfer, the contribution due to the inversion-site grating is always less than 5% of the total

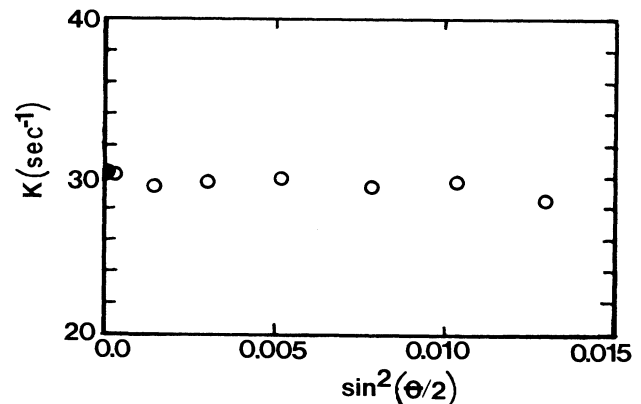


FIG. 2. Grating decay rate vs write-beam crossing angle for FWM in Cr^{3+} ions in inversion sites in alexandrite at 30 K. The solid point is twice the fluorescence decay rate.

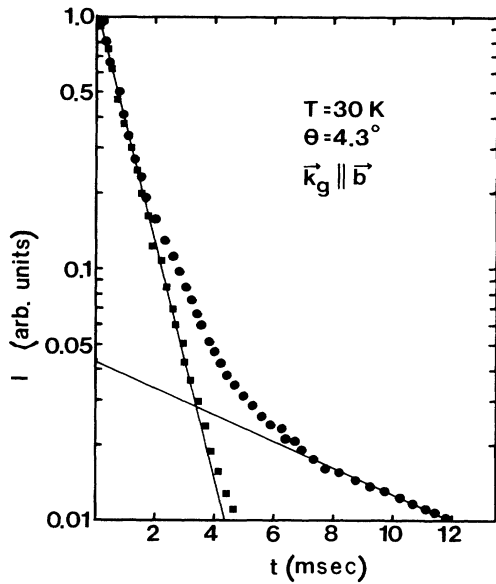


FIG. 3. FWM signal intensity vs time for Cr^{3+} ions in mirror sites in alexandrite at 30 K.

signal and thus the error incurred by the use of this crude separation technique does not greatly affect the accuracy of the diffusion coefficient determined from these measurements as discussed below.

The values of the decay rates obtained in this way are shown plotted versus $\sin^2(\theta/2)$ in Fig. 4 for several temperatures. Above 150 K, no angular variation of K is observed as reported previously.⁴ The data shown in Fig. 4 were obtained with the laser beams aligned so that the

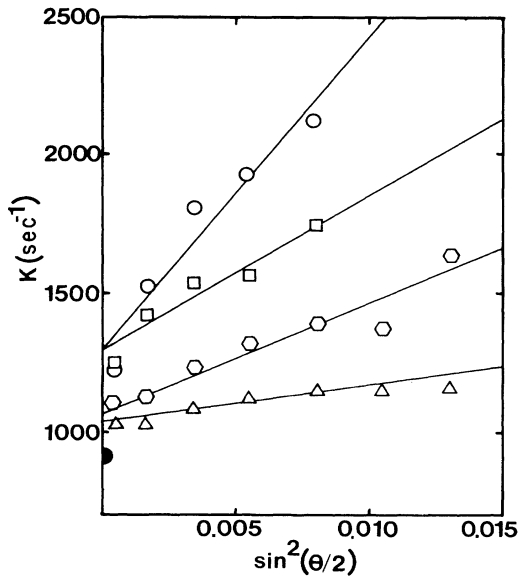


FIG. 4. Grating decay rate vs write-beam crossing angle for FWM in Cr^{3+} ions in mirror sites in alexandrite at several temperatures for 50 mW total write-beam laser power. Circles, 6 K; squares, 15 K; hexagon, 30 K; triangles, 60 K. The solid point represents twice the fluorescence decay rate. (See text for explanation of theoretical curves.)

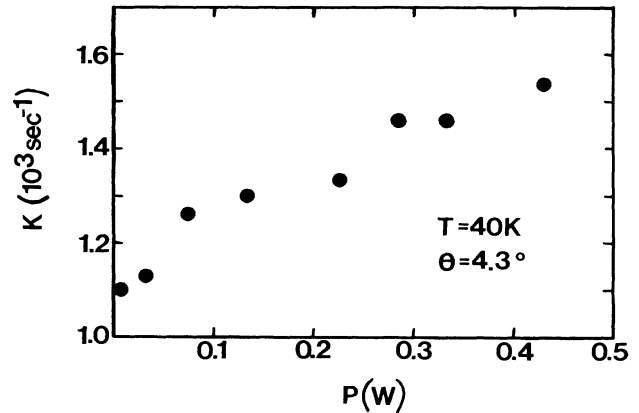


FIG. 5. Grating decay rate vs write-beam laser power at 40 K for Cr^{3+} ions in mirror sites in alexandrite at $\theta=4.3^\circ$.

grating wave vector was parallel to the crystallographic b axis. When similar measurements were made at low temperatures with the beams aligned so that the grating wave vector was parallel to the c axis, the observed variation of K with θ was much weaker.

One interesting aspect of the data shown in Fig. 4 is that the curves each extrapolate to values at $\theta=0^\circ$ which are greater than the measured values of twice the fluorescence decay rates, $2/\tau$. Although these measurements were made at low laser powers in order to minimize effects of local heating, the discrepancy in the $\theta=0^\circ$ value of K may be associated with the power dependence of the grating decay rate. Figure 5 shows the variation of K with laser power at 40 K for a crossing angle of 4.3° . No change was observed in the fluorescence lifetime as a function of laser excitation power. The increase in K with laser power indicates the presence of power-dependent effects that are not included in Eq. (1). Figure 6 shows the variation of FWM scattering efficiency with the square of the laser power in the write beams at 40 K for three crossing angles. The observed linear dependences are consistent with the room-temperature results reported earlier⁴ and are consistent with theoretical predictions of laser interaction with a two-level atomic system.

The diffusion coefficient obtained from fitting Eq. (1) to the slope of curves such as those shown in Fig. 4 is plotted versus temperature in Fig. 7. The values obtained for D are zero above 150 K and increase as $T^{-1/2}$ to about $4.2 \times 10^{-7} \text{ cm}^2 \text{ sec}^{-1}$ at 6 K. From these values, the diffusion length can be determined using the relationship $L_d = (2D\tau)^{1/2}$. The values obtained for L_d and D are listed in Table I.

B. Interpretation of results

To interpret the data presented above, we need to obtain a theoretical estimate for the magnitude of D including its directional dependence, a model for explaining the relative change of D with temperature, and a model for explaining the variation of D with laser power.

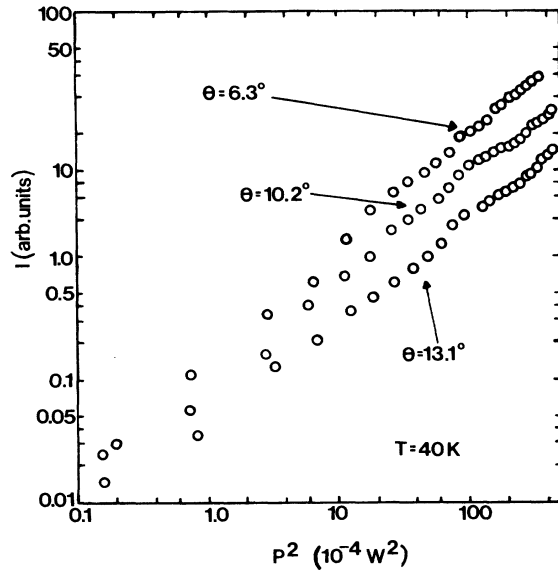


FIG. 6. FWM signal intensity of Cr^{3+} ions in mirror sites in alexandrite as a function of the square of the laser power of the write beams at 40 K.

The diffusion coefficient for exciton migration can vary with temperature due to various types of exciton-phonon interaction processes. For the temperature range of interest here, phonon absorption to higher-energy levels with stronger oscillator strengths is negligible^{2,3} and the population of optical phonons at temperatures much less than the Debye temperature is very small. Exciton scattering by acoustic phonons⁸ predicts a temperature dependence of the type shown in Fig. 7. For this long-mean-free-path model the diffusion coefficient can be expressed as⁸

$$D = \frac{1}{6} \langle \tau_s v^2 \rangle \approx \frac{1}{6} \langle \tau_s \rangle \langle v^2 \rangle, \quad (2)$$

where $\langle \tau_s \rangle$ is the mean scattering time and $\langle v^2 \rangle$ is the mean-square group velocity of the excitons. The scattering time can be separated into a contribution due to acoustic phonons and a contribution due to exciton scattering from all other sources such as surfaces, crystal defects, and optic phonons.

$$\tau_s^{-1} = \tau_{\text{ph}}^{-1} + \tau_0^{-1}. \quad (3)$$

The exciton-acoustic-phonon scattering time varies with

TABLE I. Energy-transfer parameters at 6 K for Cr^{3+} ions in mirror sites in alexandrite.

| | |
|---|-----------------------|
| N_m (cm^{-3}) | 8.9×10^{18} |
| τ_i (msec) | 63.2 |
| τ_m (msec) | 2.4 |
| D ($\text{cm}^2 \text{sec}^{-1}$) | 4.20×10^{-7} |
| D_{theory} ($\text{cm}^2 \text{sec}^{-1}$) | 1.80×10^{-7} |
| L_d (cm) | 4.5×10^{-5} |

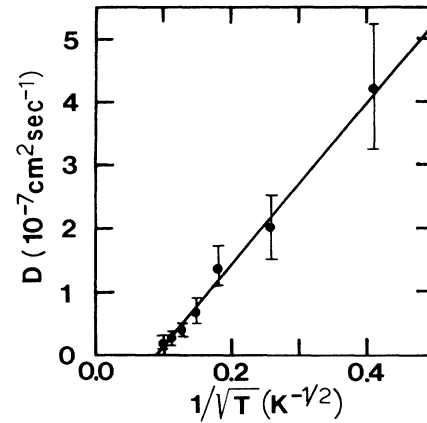


FIG. 7. Temperature dependence of the exciton-diffusion coefficient for Cr^{3+} ions in the mirror sites in alexandrite. (See text for explanation of theoretical line.)

temperature as $\tau \propto T^{-1/2}$ in the temperature range of interest, whereas the other scattering processes have a variety of different temperature dependences.⁸ If the acoustic-phonon scattering time is much shorter than the scattering time for other processes, Eq. (3) can be expanded to give

$$\tau_s \approx \tau_{\text{ph}} - \tau_{\text{ph}}^2 / \tau_0, \quad (4)$$

and Eq. (2) has the form

$$D = AT^{-1/2} - B, \quad (5)$$

where A is a constant involving the exciton velocity and the matrix element for exciton-acoustic-phonon scattering. B contains a ratio of the rates of exciton scattering by acoustic phonons and by all other centers. The temperature dependence of B is unknown, but the solid line in Fig. 7 is consistent with Eq. (5), assuming B to be independent of temperature. This gives an excellent fit between theoretical predictions and experimental results.

The magnitude of the diffusion coefficient found from these experiments at low temperature is much greater than expected for exciton migration among randomly distributed Cr^{3+} ions with the level of concentration present in our sample. It is difficult to derive a theoretical estimate for D in the long-mean-free-path model since the details of the shape of the exciton band are not known. However, a rough theoretical estimate can be obtained for D by considering the rate of energy transfer between two Cr^{3+} ions. The mechanism of energy migration among Cr^{3+} ions in ruby crystals has been identified as exchange interaction.^{9,10} In the simplest model for direct exchange, the energy-transfer rate between two ions separated by a distance R is given by¹¹

$$P(R) = (2\pi\Omega Z^2 / \hbar) \exp(-2R/L) \\ = P_0 \exp(-2R/L), \quad (6)$$

where Z depends on the spatial overlap of the electron wave functions, L is the average Bohr radius of the wave function, and the spectral overlap integral Ω includes the product of the normalized emission spectrum of the sensitizer ion ϵ_s and the normalized absorption spectrum of the activator ion α_a . For ruby, the value of P_0 has been estimated to be¹² $4.3 \times 10^{14} \text{ sec}^{-1}$. For multistep energy migration, the diffusion coefficient can be expressed in terms of the ion-ion interaction rate as¹³

$$D = \frac{1}{6} \int_0^\infty R^2 P(R) \rho(R) dR, \quad (7)$$

where the probability density of finding an ion at the distance R from the ion at the origin is given by¹³

$$\rho(R) = 4\pi N_m R^2 \exp(-4\pi N_m R^3/3). \quad (8)$$

The diffusion coefficient then becomes

$$D = (2\pi N_m P_0/3) \int_a^\infty R^4 \exp\{-[(2R/L) + (4\pi N_m R^3/3)]\} dR. \quad (9)$$

The lower limit of the integral is taken to be $a = 2.7 \text{ \AA}$, which is the smallest distance between Cr^{3+} ions in mirror sites. L is always close to 1 \AA and has been estimated for ruby⁹ to be 0.97 \AA . This value for L , along with $N_m = 8.9 \times 10^{18} \text{ cm}^{-3}$ for the concentration of mirror-site ions in our sample, can be used in Eq. (9) and the integral evaluated numerically to give $2.23 \times 10^{-41} \text{ cm}^5$. Using this and the ruby value for P_0 gives a value for the diffusion coefficient of $1.8 \times 10^{-7} \text{ cm}^2 \text{ sec}^{-1}$, which is a factor of about 2.35 smaller than the diffusion coefficient obtained from analyzing the low-temperature FWM results. This represents excellent agreement between the magnitudes of D determined experimentally and theoretically, especially considering that Eq. (9) is strictly applicable for hopping migration and thus underestimates D for long-mean-free-path migration. In addition, nonuniform distributions of the Cr^{3+} ions can enhance the energy transfer enough to account for differences in the experimental and theoretical values of D . The effective diffusion coefficient in heavily doped ruby has been reported to be 2 orders of magnitude greater than the value found here for alexandrite.¹⁴ Scaling for the difference in concentration brings these two results into agreement.

The fact that the diffusion coefficient for energy migration in the c direction is about an order of magnitude smaller than for migration in the b direction may be attributed to the anisotropy of the ion-ion interaction, or it may be associated with a nonuniform spatial distribution of Cr^{3+} ions since chromium-ion banding in c planes is known to be present in alexandrite crystals.¹⁵

The magnitude of the grating decay rate and its increase with laser power at low temperatures are more difficult to understand. The facts that the fluorescence decay rate is independent of power while the values of K at $\theta = 0^\circ$ are greater than $2/\tau$ at low temperatures where diffusion is taking place but equal to $2/\tau$ at high temperatures, indicate that at high laser power there is an additional process that contributes to the decay of the grating without shortening the metastable-state lifetime. It is im-

portant to note that the fluorescence lifetimes measured with crossed-laser-beam excitation (identical conditions to grating decay measurements) are the same as those measured with standard single-beam excitation. Nonlinear diffusion and relaxation processes which could lead to the observed power dependence would also produce nonexponential decays in the fluorescence, which were not observed. One way to explain these observations is to postulate the presence of exciton trapping at centers which have fluorescence properties similar to the mirror-site ions but which have no difference in their complex refractive index when they are in the excited state instead of the ground state. These would act as quenching centers for the grating but not the fluorescence, while enhanced trapping through exciton-exciton or exciton-phonon processes could provide the observed power dependence of the grating decay rate. Finally, it should be pointed out that the simple expression given for K in Eq. (1) is strictly valid only for a limited region of the relative strength of the exciton scattering rate compared to the ion-ion interaction rate.¹⁶ For values of these parameters outside of the allowed region, the exact expression for the dependence of K on θ deviates from a simple straight line at small values of θ and can actually be made to fit the low-temperature data shown in Fig. 4 with the measured value for $2/\tau$ at $\theta = 0^\circ$. The usefulness of such a fit is limited at the present time by the lack of knowledge of the microscopic interaction parameters. This will be the subject for future investigations.

A similar discrepancy between the grating decay rate at zero crossing angle and twice the fluorescence decay rate was observed in FWM experiments on ruby crystals with high Cr^{3+} concentrations⁶ and was attributed to the presence of exchange-coupled pairs of Cr^{3+} ions. No energy migration was observed by FWM measurements in heavily doped ruby. In alexandrite, the pairs are present even at low Cr^{3+} concentrations due to the nonuniform distribution effects.² It is not clear at the present time what role these pairs play in the grating dynamics, but their effects on the FWM results in concentrated ruby indicate that they may be responsible for the enhanced FWM signal decay and its power dependence observed in alexandrite at low temperatures.

IV. FWM MEASUREMENT OF DEPHASING TIME

The standard theoretical formalism used to interpret FWM signals is based on the interaction of three laser beams with a two-level atomic system.¹⁷⁻¹⁹ Although there have been some attempts to extend the theory to account for the presence of additional levels of the atomic system, the results become extremely complicated and no model has been developed that is generally useful in the interpretation of experimental data. For the FWM experiments on alexandrite described here, the laser write beams interact directly with the ${}^4A_{2g} \rightarrow {}^4T_{2g}$ transition of the Cr^{3+} ions. Fast radiationless relaxation occurs to the 2E_g metastable state. The laser-induced population grating will be made up of ions in both the unrelaxed ${}^4T_{2g}$ level and the 2E_g metastable state. In general, it is difficult to separate the contributions to the FWM signal due to the two types

of population gratings. Most of the FWM characteristics will be associated with the metastable state due to its greater population. However, the dephasing of an atomic system driven by coherent laser beams is generally associated with the unrelaxed excited state of the atomic transition in resonance with the laser frequency. Thus, in the alexandrite experiments described here, the dephasing time T_2 of the FWM signal should be attributed to phonon scattering and relaxation processes occurring in the ${}^4T_{2g}$ level. We describe below an analysis of the FWM scattering-efficiency data obtained on alexandrite, which results in the determination of the dephasing time of the ${}^4T_{2g}$ level. The normal two-level system model for FWM is used in this analysis since no appropriate multilevel model is available. Thus the results should be taken as a qualitative demonstration of the analysis technique, and the quantitative values should be considered as only approximations to the physical quantities. The comparison of the results of our analysis with values of the same parameters obtained by other experimental methods discussed below shows that the two-level model provides a

good approximation for this case. It should also be pointed out that recent accumulated photon-echo experiments on Nd^{3+} ions in glass have also used this type of two-level model to determine the radiationless relaxation time of a multilevel atomic system.²⁰

The exact dependence of the FWM signal efficiency with the crossing angle of the write beams varies with the relative contributions to the laser-induced grating from the modulation of the absorption and dispersion components of the complex refractive index, $\Delta\alpha$ and Δn , respectively. The dephasing time of the atomic system depends on the ratio of these modulation depths. Thus, analyzing the angular dependence of the FWM signal efficiency provides a method for determining T_2 .

A. Computer modeling of $\eta(\theta)$

Using the master-equation approach, the polarization of a two-level system in resonance with a laser driving field can be derived to be¹⁷⁻¹⁹

$$\tilde{P} = (\tilde{\mu}^2 \Delta N_0 T_2 \mathbf{E} / \hbar) \{ [\sin(\omega t) + (\omega_{21} - \omega) T_2 \cos(\omega t)] [1 + (\omega - \omega_{21})^2 T_2^2 + 4\Omega^2 T_2 \tau]^{-1} \} + \xi \mathbf{E} \cos(\omega t). \quad (10)$$

The first term represents the contribution due to the atomic transition near resonance with the laser frequency, while the second term (ξ) represents the combined effects of all other transitions in the sample.²¹ Here, $\tilde{\mu}$ is the dipole moment of the transition, ΔN_0 is the average equilibrium density of the population difference between the ground and excited states, τ is the fluorescence decay time of the excited state, E is the electric field of the laser beams in the crystal, ω is the angular frequency of the laser, ω_{21} is the resonant frequency of the atomic transition, and $\Omega = \tilde{\mu} E / (2\hbar)$ is the precession frequency of the dipole moment. The polarization can be used to obtain the complex susceptibility

$$\chi = (\tilde{\mu}^2 \Delta N_0 T_2 / \hbar) \{ [T_2(\omega_{21} - \omega) - i] \times [1 + (\omega - \omega_{21})^2 T_2^2 + 4\Omega^2 T_2 \tau]^{-1} \} \xi. \quad (11)$$

The information concerning the physical characteristics of the system pertaining to absorption, dispersion, FWM, and saturation are contained in χ .

In cgs units, the wave equation describing the propagation of the laser beams in the atomic system is

$$\nabla^2 \mathbf{E} = (\mu/c^2) \frac{\partial^2 \mathbf{E}}{\partial t^2} + (4\mu\pi/c^2) \frac{\partial^2 \mathbf{P}}{\partial t^2}. \quad (12)$$

The electric fields of the laser beams can be described as plane waves,

$$\mathbf{E}_i(\mathbf{r}, t) = (\mathbf{A}_i/2) \exp[-i(\omega_i t - \mathbf{k}_i \cdot \mathbf{r})] + \text{c.c.}, \quad i = 1-4. \quad (13)$$

For degenerate FWM, all ω_i are equal, all $|\mathbf{k}_i| = k$, and, to satisfy the Bragg scattering condition, $\sum_i \mathbf{k}_i = 0$. If \mathbf{E}_1 and \mathbf{E}_2 represent the write beams, the read beam \mathbf{E}_3 is counterpropagating to \mathbf{E}_1 and the signal beam \mathbf{E}_4 is counterpropagating to \mathbf{E}_2 . To simplify the mathematical expressions, degenerate FWM is assumed. This will thus be only an approximation of our experimental condition in which the read beam had a different frequency than the write beams. Rough calculations using the exact read-beam frequency indicate that negligible error is introduced by this simplification as long as the read beam is weak enough that it does not affect the population grating. In addition, we make several assumptions relevant to our experimental conditions. The write beams are assumed to be more intense than the read and signal beams, the signal beam is assumed to be weaker than the read beam, and it is assumed that the weak beams have no beam depletion. Substituting the polarization and field expressions into the wave equation, using the "slowly varying envelope approximation," and equating like k -vector exponentials, a set of coupled, complex, differential equations are obtained. The scattering efficiency is defined as $\eta = |A_4|^2 / |A_3|^2$, where the A_i represent the amplitudes of the beams. It is common practice to work with the normalized scattering efficiency, which depends only on A_4 . In this case we need to consider only the coupled equations for A_2 and A_4 , which can be separated into real and imaginary parts. Their variation with the write-beam crossing angle in the crystal θ is given by

$$\frac{dA_2^i}{d\theta} = [(A_2^r D_1^r - A_2^i D_1^i - A_2^r D_2^r - A_2^i D_2^i) k_1 \csc(\theta/2) - (D_2^r A_4^r - D_2^i A_4^i) (k_3^2/k_1) \csc(\theta/2)]/2, \quad (14)$$

$$\frac{dA_2^r}{d\theta} = [(-A_2^i D_1^r - A_2^r D_1^i + A_2^i D_2^r - A_2^r D_2^i) k_1 \csc(\theta/2) - (D_2^i A_4^r + D_2^r A_4^i) (k_3^2/k_1) \csc(\theta/2)]/2, \quad (15)$$

$$\frac{dA_4^i}{d\theta} = [(-A_4^r D_1^r + A_4^i D_1^i + A_4^r D_2^r + A_4^i D_2^i) k_3 \csc(\theta/2) + (D_2^r A_2^r - D_2^i A_2^i) (k_1^2/k_3) \csc(\theta/2)]/2, \quad (16)$$

$$\frac{dA_4^r}{d\theta} = [(A_4^i D_1^r + A_4^r D_1^i - A_4^i D_2^r + A_4^r D_2^i) k_3 \csc(\theta/2) + (D_2^i A_2^i + D_2^r A_2^r) (k_1^2/k_3) \csc(\theta/2)]/2, \quad (17)$$

where the superscripts r and i refer to real and imaginary, respectively, and the coupling coefficients are

$$D_1 = D_1^r + iD_1^i = 2\pi\mu R(\kappa - \xi), \quad (18)$$

$$D_2 = D_2^r + iD_2^i = \pi\mu R \Delta\kappa. \quad (19)$$

Here, R is the distance from the center of the overlap region of the beams, μ is the permeability of the material, κ is a complex parameter related to the complex index of refraction, and $\Delta\kappa$ is the laser-induced modulation in this parameter. The latter parameters are given by¹⁷⁻¹⁹

$$\kappa = \alpha_0(i + \delta)(1 + \delta^2)(1 + \delta^2 + |E/E_s|^2)^{-2}, \quad (20)$$

$$\Delta\kappa^* = 2|E/E_s|^2[\alpha_0(i + \delta)](1 + \delta^2 + |E/E_s|^2)^{-2}, \quad (21)$$

where the detuning parameter is $\delta = (\omega - \omega_{12})T_2$, α_0 is the peak absorption coefficient, and E_s is the saturation field. The detuning parameter which accounts for the width of the resonant electronic transition contains the frequency dependence of the results. For laser fields much smaller than the saturation field, $\kappa \approx \chi + \xi$ and $\Delta\kappa^* \approx \Delta\chi$.

It is not possible to obtain a general analytic solution for η which has a simple enough form to be useful in fitting experimental data.⁷ In order to understand the variation of scattering efficiency with write-beam crossing angle, it is necessary to either make several simplifying assumptions or to resort to numerical solutions. We compare here the results of both approaches.

Equations (14)–(16) can be solved numerically using a fourth-order Runge-Kutta method. Treating the real and imaginary parts of both coupling parameters as adjustable parameters, curves with various shapes can be obtained. Three examples are shown in Fig. 8. Although each of these show the FWM scattering efficiency rising sharply to a peak value and then decreasing at larger angles, the exact position of the peak and the rate of decrease with crossing angle vary greatly with choice of coupling parameters. The peak shifts to higher angles and the curve shape becomes broader as D_2^r or D_2^i are increased, whereas increases in D_1^r or D_1^i have the effect of raising the scattering efficiency at larger angles. The values of the components of the coupling parameters are related to the laser-induced modulations of the absorption and dispersion parts of the refractive index by

$$\Delta\alpha = (4\pi\omega/nc) \text{Im}(\chi) = -2\alpha D_2^i/D_1^i, \quad (22)$$

$$\Delta n = (2\pi/n) \text{Re}(\chi) = (ac/\omega) D_2^r/D_1^i, \quad (23)$$

where α is the average absorption coefficient of the ma-

terial at the write-beam wavelength, ω . Thus as Δn or $\Delta\alpha$ increases, the peak of the curve shifts to higher angles, and an increase in α increases η at larger angles.

To obtain an approximate expression for $\eta(\theta)$, Eqs. (12)–(14) can be linearized by making the substitution $t = 2 \ln[\tan(\theta/4)]$. Then the secular equation can be solved to obtain solutions for different special cases. For example, if

$$(D_2^i)^2 + (D_2^r)^2 - (D_1^i + D_2^i)^2 > 0$$

and

$$|D_1^r - D_2^r| \neq \begin{cases} 0 \\ [(D_2^i)^2 + (D_2^r)^2 - (D_1^i + D_2^i)^2]^{1/2}, \end{cases}$$

the solution is

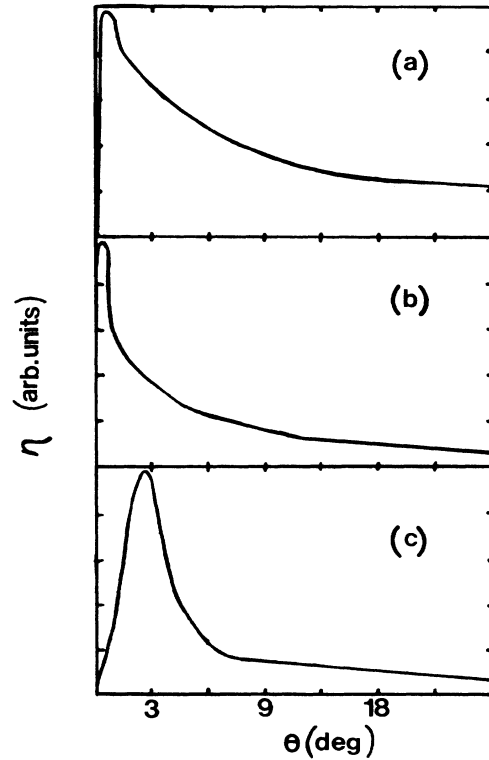


FIG. 8. Computer-generated plots of the FWM scattering efficiency vs the write-beam crossing angle for different values of the coupling parameters. (a) $D_1^r = 0.005$, $D_1^i = 0.100$, $D_2^r = 0.125$, and $D_2^i = 0.00002$. (b) $D_1^r = 0.006$, $D_1^i = 0.025$, $D_2^r = 0.090$, and $D_2^i = 0.00002$. (c) $D_1^r = 0.005$, $D_1^i = 0.075$, $D_2^r = 0.188$, and $D_2^i = 0.000096$.

$$\eta(\theta) = 2[(D_2^i)^2 + (D_2^r)^2][(D_2^i)^2 + (D_2^r)^2 - (D_1^i + D_2^i)^2]^{-1} \sin^2\{k[(D_2^i)^2 + (D_2^r)^2 - (D_1^i + D_2^i)^2]^{1/2} \ln[\tan(\theta/4)]\}. \quad (24)$$

For the appropriate choices of the coupling parameters, Eq. (24) gives curves similar to those shown in Fig. 8. Other special cases will have significantly different forms for the solution of the coupled differential equations, but they predict the same general dependence of η on θ .

The advantage of the analytic solution is that it provides some insight into the origin of the angular dependence of the FWM scattering efficiency. The factor containing θ in the expression shown in Eq. (24) is related to the interaction length of the read beam with the grating, and the additional parameters in the argument of sine function describe the density of the grating fringes and the grating modulation depth. Evidently, it is the variation of these parameters that determines the shape of the curves of $\eta(\theta)$. The disadvantages of the analytic solution are that it is difficult to justify the assumptions necessary to define a specific case, and it is not possible to independently determine values for Δn and $\Delta\alpha$. Both of these disadvantages are overcome by using the numerical method of solution.

B. Interpretation of results

The numerical method for solving Eqs. (14)–(17) was applied to experimental data obtained on alexandrite and ruby crystals. Figure 9 shows the measured values of

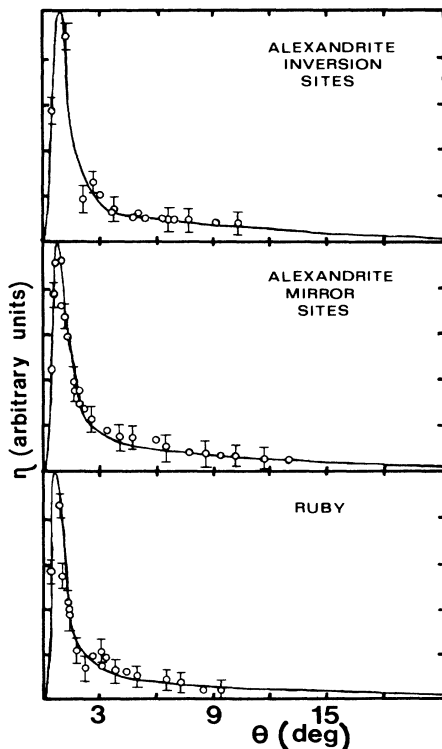


FIG. 9. FWM signal efficiency vs the write-beam crossing angle at 300 K for Cr^{3+} ions in the mirror sites and inversion sites in alexandrite and in ruby. (See text for explanation of theoretical lines.)

FWM scattering efficiency versus write-beam crossing angle for Cr^{3+} ions in both types of crystal-field sites in alexandrite and in ruby. The solid lines represent the best fits to the data using the numerical-solution technique and a nonlinear-regression least-squares-fitting routine, with the real and imaginary components of the coupling coefficients treated as adjustable parameters. The results were found to be independent of temperature between 30 and 300 K. The fitting parameters were substituted into Eqs. (22) and (23) to obtain values for the laser-induced modulation depths due to changes in absorption and dispersion. The values obtained from this procedure are listed in Table II.

Once these parameters are known, Eq. (21) can be solved for the dephasing time of the atomic system,

$$T_2 = (2\omega/c)(\Delta n/\Delta\alpha)(\omega - \omega_{12})^{-1}. \quad (25)$$

The values of T_2 obtained for ruby and alexandrite are given in Table II.

For the two materials investigated here, the theoretical fitting of the angular dependence of the FWM scattering efficiency is very sensitive to changes in D_2^i but very insensitive to changes in D_2^r , since the magnitude of the latter parameter is very small. This results in an accurate determination of Δn but not $\Delta\alpha$. Previous approaches to calculating these components of the modulation depths provide an accurate method for determining $\Delta\alpha$ but not Δn .^{19,22} The calculation of $\Delta\alpha$ based on a two-level system gives^{4,19}

$$\Delta\alpha = N_0 I_0 \sigma_1 (\sigma_2 - \sigma_1) (2I_0 \sigma_1 + h\nu/\tau)^{-1}, \quad (26)$$

where N_0 is the concentration of active ions, I_0 is the energy density of the write beams with photon energy $h\nu$, and σ_1 and σ_2 are the ground- and excited-state absorption cross sections, respectively. Since excited-state absorption measurements have been made for both ruby²³ and alexandrite,²⁴ it is possible to obtain an accurate value of $\Delta\alpha$ using Eq. (26). The error bars listed in Table II are associated with estimates of the parameters used in Eq. (26) as well as with the curve-fitting procedure used to determine the coupling parameters.

TABLE II. FWM measurements of dephasing times in alexandrite and ruby at room temperature.

| Parameter | Alexandrite | | Ruby |
|-------------------------------------|-----------------------|-----------------------|-----------------------|
| | Inversion sites | Mirror sites | |
| α (cm^{-1}) | 0.36 | 1.05 | 1.37 |
| I_0 (W/cm^2) | 60 | 50 | 60 |
| η | 10^{-4} | 10^{-4} | 10^{-4} |
| $\Delta\alpha$ (cm^{-1}) | 1.10×10^{-3} | 1.90×10^{-2} | 1.06×10^{-2} |
| Δn | 2.52×10^{-5} | 1.83×10^{-5} | 8.16×10^{-5} |
| T_2 (psec) | 80 ± 5 | 2.2 ± 4 | 4.5 ± 3 |
| ΔE (cm^{-1}) | 6400 | 800 | 2300 |

The transverse relaxation time T_2 is related to the lifetime of the excited level T_1 and the pure dephasing rate due to scattering events γ by

$$T_2^{-1} = (2T_1)^{-1} + \gamma. \quad (27)$$

If the fast radiationless relaxation from the ${}^4T_{2g}$ "pump band" to the 2E_g metastable state is the dominant process for dephasing the atomic system, the values determined for T_2 represent twice the relaxation times associated with this process. The value of 2.25 psec obtained in this way for T_1 in ruby is consistent with the upper limit of 7 psec found from pulse-probe measurements to be the ${}^4T_{2g}$ - 2E_g relaxation rate.²⁵ The longer dephasing time found for alexandrite inversion-site ions which have a ${}^4T_{2g}$ - 2E_g energy difference almost 3 times greater than in ruby, and the smaller dephasing time obtained for mirror-site ions in alexandrite which have a smaller energy-level difference between the pump band and metastable state, establish the existence of a relationship between the values of T_2 and the energy-level splitting of the excited states. This is shown explicitly in Fig. 10. The observed dependence of T_2 on ΔE is expected if the radiationless transitions between the ${}^4T_{2g}$ and 2E_g levels are responsible for the dephasing of the system. Measurements made on alexandrite at 30 K gave the same value for T_2 as found at 300 K, indicating that strongly temperature dependent phonon scattering processes are not important.

From the preceding discussion, it appears that the ${}^4T_{2g}$ - 2E_g relaxation process does dominate the dephasing for the FWM experiments on ruby and alexandrite. This decay process causes "lifetime broadening" of the ${}^4T_{2g}$ level. The zero-phonon lines of the lowest-lying crystal-field state of this level for ruby and the mirror-site ions in alexandrite have been observed^{3,26} at low temperatures to have linewidths of the order of 25 cm^{-1} , which is significantly greater than the predicted contributions to the linewidth of a few wave numbers obtained from the measured values of T_2 . This is due to the fact that these lines exhibit significant inhomogeneous broadening due to the

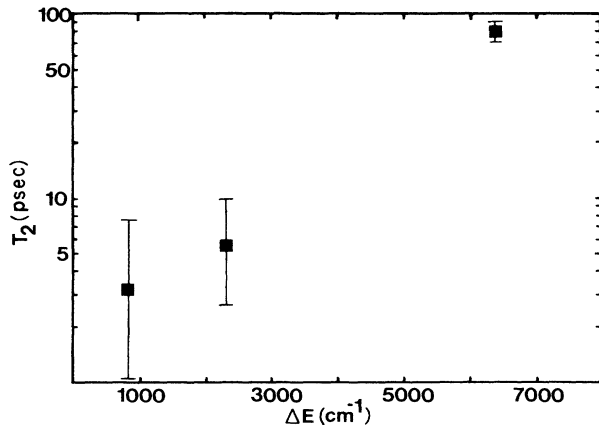


FIG. 10. Variation of dephasing time obtained from analysis of FWM measurements with the energy-level splitting of the ${}^4T_{2g}$ and 2E_g levels for Cr^{3+} ions in alexandrite and ruby.

sensitivity of the ${}^4T_{2g}$ level to the local crystal field. Since these lines appear on the side of the broad vibronic band, it is difficult to accurately deconvolute the homogeneous and inhomogeneous contributions to the line shape.

These results imply that the ${}^2T_{1g}$ levels lying between the ${}^4T_{2g}$ and 2E_g levels do not play a significant role in the pump-band-to-metastable-state relaxation process. This is consistent with previous theoretical predictions.²⁷

V. DISCUSSION AND CONCLUSIONS

The observation of long-range energy migration among the mirror-site Cr^{3+} ions in alexandrite at low temperatures is a surprising result. Attempts to observe energy migration in ruby using FWM techniques have been repeated several times without success.^{6,28,29} The observed energy-transfer characteristics are consistent with having a higher concentration of Cr^{3+} ions than predicted by assuming a uniform distribution of mirror-site ions. An increase by about a factor of 2.35 in the local density of Cr^{3+} ions over the average concentration will account for the observed characteristics. This is not unreasonable because of the chromium-ion banding that occurs in planes perpendicular to the direction of crystal growth in alexandrite.¹⁵ Also, it should be emphasized that the simple exchange model used in Sec. III to analyze the FWM results underestimates the strength of the ion-ion interaction causing the energy transfer. The superexchange model used to explain transfer in ruby provides an interaction mechanism that is stronger and more directional than direct-exchange interaction.^{9,10} Developing a superexchange model for ion-ion interaction in alexandrite is an important problem for future theoretical work.

The lack of any observed long-range energy transfer among the inversion-site Cr^{3+} ions is consistent with the lower concentration of these ions compared to the mirror-site ions. The evidence of enhanced energy transfer from mirror-site to inversion-site ions at low temperature is consistent with the results of time-resolved, site-selection spectroscopy measurements reported previously.² The temperature range in which nonexponential grating decays are observed is the same as the temperature range in which site-selection spectroscopy results show enhanced energy transfer to occur. The rate of diffusion-controlled energy transfer is given by

$$W_{mi} = 4\pi DR_i N_i, \quad (28)$$

where R_i and N_i are the exciton-trapping radius and concentration of inversion-site ions. Using the nearest-neighbor distance between an inversion- and mirror-site ion for R_i and the diffusion coefficient found from FWM measurements, the transfer rate at 6 K is estimated to be of the order of $3 \times 10^5 \text{ sec}^{-1}$. This value is consistent with the energy-transfer rate at 10 K determined by the site-selection spectroscopy measurements reported in Ref. 2 if the average separation between a mirror-site and inversion-site ion is about 12 Å. It is difficult to determine an accurate value for the average separation between mirror-site and inversion-site ions due to the nonuniform distribution of Cr^{3+} ions discussed previously. However, there appears to be both quantitative and qualitative

agreement in the results on energy transfer between mirror- and inversion-site ions obtained by the two different types of experimental techniques.

The investigation of the FWM scattering efficiency on the crossing angle of the write beams described here is important for two reasons. First, it demonstrates a method for determining the contributions to the laser-induced refractive-index gratings due to absorption changes and to dispersion changes. It is difficult to determine the relative contributions from these two types of gratings using other techniques. Second, it provides a measurement of the dephasing time of an atomic system driven by laser sources. Other coherent transient techniques for obtaining T_2 , such as photon-echo measurements, have generally been used only for probing metastable states such as the 2E_g level of ruby³⁰ where the dephasing time is much longer. The accumulated photon-echo technique recently applied to rare-earth-doped glasses²⁰ has provided the same type of information on T_2 of nonmetastable states as our experimental technique, and comparing the results of these two types of experiments on the same sample will be the subject of future research. Determination of T_2 through linewidth measurements is complicated by inhomogeneous broadening.

An important question concerning these results is the relationship between the values of T_2 determined from the analysis of the FWM data and the pump-band-to-metastable-state radiationless relaxation rate for the Cr^{3+} -doped laser crystals investigated here. This has been a parameter of interest for many years and has always been difficult to measure.^{25-27,31-42} The actual

relaxation process can be divided into several steps, including relaxation to the bottom of the vibronic potential well of the ${}^4T_{2g}$ level, crossover to an excited vibrational level of the 2E_g level, and relaxation to the bottom of the 2E_g level. The measured dephasing time may be associated with one specific step in this overall process and the total relaxation time may be longer. However, the data indicate a close relationship between these two times, especially in terms of the energy-gap dependence shown in Fig. 10 and the fact that the magnitudes of the relaxation times determined from the measured T_2 's compare favorably with those determined from other measurements. The lack of any observed temperature variation of T_2 in the range investigated is consistent with the temperature dependence expected for phonon-emission processes involving large energy gaps of the size relevant to these data. Establishing the exact relationship between T_2 and the relaxation time requires additional work with direct picosecond pulse-probe measurements which will be the subject of future work.

ACKNOWLEDGMENTS

This research was supported by the U. S. Army Research Office, and by the National Science Foundation under Grant No. DMR-82-16551. The alexandrite crystal was supplied by Allied Corporation, and the authors gratefully acknowledge helpful discussions with Dr. D. Heller and Dr. M. Shand of Allied Corporation.

- 1J. C. Walling, O. G. Peterson, H. P. Jenssen, R. C. Morris, and E. W. O'Dell, *IEEE J. Quantum Electron.* **QE-16**, 1302 (1980); J. C. Walling, D. F. Heller, H. Samelson, D. J. Harter, J. A. Pete, and R. C. Morris, *ibid.* **QE-21**, 1568 (1985).
- 2R. C. Powell, L. Xi, X. Gang, G. J. Quarles, and J. C. Walling, *Phys. Rev. B* **32**, 2788 (1985).
- 3A. B. Suchocki, G. D. Gilliland, R. C. Powell, J. M. Bowen, and J. C. Walling (unpublished).
- 4A. M. Ghazzawi, J. K. Tyminski, R. C. Powell, and J. C. Walling, *Phys. Rev. B* **30**, 7182 (1984).
- 5J. R. Salcedo, A. E. Siegman, D. D. Dlott, and M. D. Fayer, *Phys. Rev. Lett.* **41**, 131 (1978).
- 6H. J. Eichler, J. Eichler, J. Knof, and Ch. Noack, *Phys. Status Solidi A* **52**, 481 (1979).
- 7C. M. Lawson, R. C. Powell, and W. K. Zwicker, *Phys. Rev. Lett.* **46**, 1020 (1981); C. M. Lawson, R. C. Powell, and W. K. Zwicker, *Phys. Rev. B* **26**, 4836 (1982); J. K. Tyminski, R. C. Powell, and W. K. Zwicker, *ibid.* **29**, 6074 (1984).
- 8V. M. Agranovich and M. D. Galanin, *Electronic Excitation Energy Transfer in Condensed Matter* (North-Holland, Amsterdam, 1982); V. M. Agranovich and Yu. V. Konobeev *Opt. Spektrosk.* **6**, 242 (1959); **6**, 648 (1959) [*Opt. Spectrosc. (USSR)* **6**, 155 (1959); **6**, 421 (1959)]; *Phys. Status Solidi*, **27**, 435 (1968).
- 9R. J. Birgeneau, *J. Chem. Phys.* **50**, 4282 (1969).
- 10J. Koo, L. R. Walker, and S. Geschwind, *Phys. Rev. Lett.* **35**, 1669 (1975).
- 11D. L. Dexter, *J. Chem. Phys.* **21**, 836 (1953); *Phys. Rev.* **126**, 1962 (1962).
- 12G. F. Imbusch, *Phys. Rev.* **153**, 326 (1967).
- 13S. Chandrasekhar, *Rev. Mod. Phys.* **15**, 1 (1943).
- 14A. Monteil and E. Duval, *J. Phys. C* **13**, 4565 (1980).
- 15S. C. Stotlar and L. B. Edgett, in *Proceedings of the Optical Society of America Annual Meeting*, Washington, D. C., 1985 (unpublished).
- 16V. M. Kenkre and D. Schmid, *Phys. Rev. B* **31**, 2430 (1985).
- 17A. Yariv and D. M. Pepper, *Opt. Lett.* **1**, 16 (1977).
- 18R. L. Abrams and R. C. Lind, *Opt. Lett.* **2**, 94 (1978); **3**, 205 (1978).
- 19K. O. Hill, *Appl. Opt.* **10**, 1695 (1971).
- 20S. Asaka, H. Nakatsuka, M. Fujiwara, and M. Matusoka, *Phys. Rev. A* **29**, 2286 (1984); H. Nakatsuka, M. Tomita, M. Fujiwara, and S. Asaka, *Opt. Commun.* **52**, 150 (1984); M. Tomita and M. Matusoka, *J. Opt. Soc. Am. B* **3**, 560 (1986).
- 21A. Yariv, *Quantum Electronics* (Wiley, New York, 1975).
- 22K. A. Nelson, R. Cassalegno, R. J. D. Miller, and M. D. Fayer, *J. Chem. Phys.* **77**, 1144 (1982).
- 23W. M. Fairbank, Jr., G. K. Klauminzer, and A. L. Schawlow, *Phys. Rev. B* **11**, 60 (1975).
- 24M. L. Shand, J. C. Walling, and R. C. Morris, *J. Appl. Phys.* **52**, 953 (1981).
- 25S. K. Gayen, W. B. Wang, V. Petricevic, R. Dorsinville, and R. R. Alfano, *Appl. Phys. Lett.* **47**, 455 (1985).
- 26A. Misu, *J. Phys. Soc. Jpn.* **19**, 2260 (1964).

- ²⁷R. Englman, B. Champagnon, E. Duval, and A. Monteil, *J. Lumin.* **28**, 337 (1983).
- ²⁸D. S. Hamilton, D. Heiman, J. Feinberg, and R. W. Hellwarth, *Opt. Lett.* **4**, 124 (1979).
- ²⁹P. F. Liao, L. M. Humphrey, D. M. Bloom, and S. Geschwind, *Phys. Rev. B* **20**, 4145 (1979); P. F. Liao and D. M. Bloom, *Opt. Lett.* **3**, 4 (1978).
- ³⁰I. D. Abella, N. A. Kurnit, and S. R. Hartmann, *Phys. Rev.* **141**, 391 (1966).
- ³¹B. Z. Malkin, *Fiz. Tverd. Tela (Leningrad)* **4**, 2214 (1962) [*Sov. Phys.—Solid State* **4**, 1620 (1963)].
- ³²A. Kiel, in *Quantum Electronics, Proceedings of the Third International Conference, Vol. 1*, edited by P. Grivet and N. Bloembergen (Columbia University Press, New York, 1963), p. 535.
- ³³J. Brossel and J. Margerie, in *Paramagnetic Resonance, Vol. II*, edited by W. Low (Academic, New York, 1963), p. 353.
- ³⁴B. S. Tsukerblat and Yu. E. Perlin, *Fiz. Tverd. Tela (Leningrad)* **7**, 3278 (1965) [*Sov. Phys.—Solid State* **7**, 2647 (1966)].
- ³⁵P. Kisliuk and C. A. Moore, *Phys. Rev.* **160**, 307 (1967).
- ³⁶J. A. Calviello, E. W. Fisher, and Z. H. Heller, *J. Appl. Phys.* **37**, 3156 (1967).
- ³⁷S. A. Pollack, *J. Appl. Phys.* **38**, 5083 (1967); *IEEE J. Quantum Electron.* **QE-4**, 703 (1968).
- ³⁸M. Anson and R. C. Smith, *IEEE J. Quantum Electron.* **QE-6**, 268 (1970).
- ³⁹P. N. Everett, *J. Appl. Phys.* **42**, 2106 (1971).
- ⁴⁰W. H. Fonger and C. W. Struck, *Phys. Rev. B* **11**, 3251 (1975).
- ⁴¹J. E. Rives and R. S. Meltzer, *Phys. Rev. B* **16**, 1808 (1977).
- ⁴²M. Montagna, O. Pilla, and G. Viliani, *Phys. Rev. Lett.* **45**, 1008 (1980).